atmosphere

MDPI

*Article*

# Formation Mechanism of Consecutive Dense Fog Events over the Ma-Zhao Expressway in Yunnan, Southwest China, Late Autumn 2022

**Yuchao Ding [1], Dayong Wen [2,*], Xingtong Chen [1], Xuekun Yang [1] and Chang'an Xiong [1]**

[1] National Engineering Research Center of Geological Disaster Prevention in Land transportation, Broadvision Engineering Consultants Co., Ltd., Kunming 650200, China; dingyuchao2019@163.com (Y.D.)
[2] Yunnan Key Laboratory of Meteorological Disasters and Climate Resources in the Greater Mekong Subregion, Yunnan University, Kunming 650091, China
* Correspondence: wdy@ynu.edu.cn

**Abstract**

Fog is a near-surface weather phenomenon with low visibility that significantly threatens transportation safety. Understanding the spatiotemporal evolution and formation mechanisms of fog is essential for improving fog forecasting and warning services to reduce related casualties and economic losses. This study examines consecutive dense fog events with long duration and high intensity that occurred along the Ma-Zhao Expressway in northeastern Yunnan from 24 to 30 October 2022. Yunnan is a typical low-latitude plateau region in southwestern China with complex terrain and diverse climates, leading to particularly complicated fog formation processes. Correlation analysis indicates that thermal and vapor factors show stronger correlations with visibility, with correlation coefficients reaching 0.68 for vertical temperature difference and −0.63 for surface relative humidity, both significant at the 99% confidence level. These values are notably higher than those of dynamic factors such as near-surface wind speed, which yields a correlation coefficient of 0.47. The results confirm the dominant role of thermal and vapor conditions in the formation and maintenance of these dense fog events, together with favorable conditions including near-surface air saturation, weak dynamic processes, and a temperature inversion in the lower troposphere. Standardized anomaly analysis reveals obvious atmospheric anomalies during the fog episodes. A strong southerly wind anomaly appears in the lower troposphere, driven by a cyclone over the Philippines and an anomalous anticyclone east of Yunnan. This southerly transport delivers warm and moist air toward the Ma-Zhao Expressway, accompanied by a positive temperature anomaly of 1.7, standard deviations near 700 hPa and a positive specific humidity anomaly of more than 2 standard deviations in the lower troposphere. These conditions favor the development of temperature inversions and atmospheric saturation, further promoting the occurrence and persistence of consecutive dense fog events. This study clarifies the key effects of thermal and vapor conditions as well as low-level southerly wind anomalies on dense fog over the Yunnan low-latitude plateau. These conclusions deepen the understanding of fog formation mechanisms in complex plateau terrain and provide a scientific reference for fog forecasting and early warning along mountain expressways in similar low-latitude plateau regions.

**Keywords:** consecutive dense fogs; expressway; low-latitude plateau region; meteorological conditions; anomalous atmospheric circulation; southwestern China



Academic Editor: Stefano Federico

Received: 28 February 2026
Revised: 11 April 2026
Accepted: 14 April 2026
Published: 19 April 2026

## 1. Introduction

Fog is a meteorological condition where water droplets or ice crystals in the air near the ground reduce horizontal visibility to less than 10,000 m [1]. In China's National Standards, fog is classified into five grades based on visibility: thin fog reduces visibility to 10,000–1000 m, heavy fog reduces visibility to 1000–500 m, dense fog reduces visibility to 500–200 m, strong dense fog reduces visibility to 200–50 m, and extreme dense fog reduces visibility below 50 m [2]. Fog significantly impacts sea, land, and air transportation, particularly strong dense fog with visibility less than 200 m, often leading to freeway closures, air traffic take-off and landing difficulties, and suspension of sea transportation. Additionally, operational management experience on highways indicates that among all adverse weather conditions, dense fog poses the greatest threat to highway operations [3].

Numerous transportation accidents occur annually due to fog, for instance, on 15 November 2017, at 07:50, over 30 vehicles collided in a chain reaction on the Chuxin Expressway in Yingshang, Fuyang, Anhui, resulting in 18 fatalities and 21 severe injuries. Some traffic meteorological stations along the expressway reported visibility below 50 m. Understanding the spatiotemporal evolution characteristics and formation mechanisms of fog is crucial for enhancing fog warning and forecasting capabilities to mitigate related human and property losses. Many researchers have thus delved into studying the phenomenon of fog for this purpose.

In terms of the spatiotemporal variation characteristics of fog, Lee et al. [4] studied the detailed spatial and temporal characteristics of various types of fog occurrence in South Korea based on empirical orthogonal function and wavelet analyses. Shrestha et al. [5] investigated the variation trend of winter fog occurrence frequency in the Nepal Terai region using airport visibility data from 1980 to 2015. In mainland China, fog days exhibit significant interdecadal, interannual, and seasonal variations. The geographical distribution of fog days shows a basic climatic feature of more in the southeast and southwest, less in the northwest [6,7]. In recent decades, the frequency of fog days in China has shown an increasing trend before 1980 and a decreasing trend after 1990, consistent with the trend of decreasing near-surface relative humidity caused by climate warming [8]. Seasonally, most parts of China experience more fog events in autumn and winter, and fewer in spring and summer, while coastal areas have more fog events in spring and summer [9]. Many scholars have conducted related studies on the characteristics of dense fog in different regions of China, such as Xinjiang Uygur Autonomous Region [10], Hebei Province [11], Shaanxi Province [12], Jiangxi Province [13] and Jiangsu Province [14,15].

The interactions among several factors, including aerosols, microphysics, moisture, radiation, and turbulence, cause fog to form, develop, and dissipate [1,16–18]. Factors such as weak cold air invasion, radiative cooling, sufficient water vapor supply, and inversion layer structure play crucial roles in fog formation and enhancement. According to Dhangar et al. [19], radiative cooling at the top and along the surface of the fog encourages vertical development of fog and increases supersaturation. Differences in the duration, time and vertical extent of fog formation at nearby stations can result from different cooling rates [20]. Radiative cooling in cases of large-scale fog is outweighed by moisture advection [21]. Pu et al. [22] discovered that the advection of moisture in two layers contributes to the intensification and persistence of fog. A strong inversion layer often accompanies the formation of dense fog [22,23]. Lower-level cold advection and upper-level warm advection promote the development of fog and enhance inversion intensity [24]. Fog intensification and formation are facilitated by adequate turbulence [25,26]. Moisture and heat exchange within the planetary boundary layer promote the downward mixing of cold air and vapor, which can support droplet formation and condensation [24,27]. Some studies have stressed the indirect effects of aerosols and hygroscopic aerosols in significant fog events [28–31].

Regarding fog dissipation, the invasion of cold air and ground warming are important mechanisms for the dissipation of fog [32–34]. Li et al. [35] have shown that deep weak moisture convergence is more important than the saturation of moisture itself, and ground heat flux promotes the occurrence of dense fog in the early stages but inhibits it in the later stages.

Due to the significant impact of dense fog on the safe operation of highways, some scholars have conducted research specifically on foggy weather along highways. For example, Tian and Wang [36] analyzed the climatic characteristics and meteorological conditions of fog along the Beijing–Tianjin–Tanggu Expressway, highlighting the significance of meteorological elements such as surface temperature, relative humidity, and wind speed in fog forecasting. Wu et al. [37] analyzed the large-scale circulation background and distribution characteristics of meteorological elements during fog events using data from automatic weather stations along the Beijing–Tianjin–Tanggu Expressway. Studies on fog monitoring, forecasting, low visibility evolution, and local dumpling fog events along the Shanghai–Nanjing Expressway have also been conducted [38–40]. The eastern coastal region of China is influenced by dual airflows from the ocean and land, resulting in the impact of both sea fog and inland fog [41,42]. Therefore, research and discussions on severe fog weather conditions along coastal highways have also been a focal point for some scholars [43,44].

Yunnan is situated in a low-latitude plateau region in southwestern China, characterized by unique geographical features, complex terrain, and a diverse climate that ranges from tropical to temperate. Within China, regions sharing similar low-latitude plateau attributes include southern Sichuan Province, western Guizhou, and western Guangxi Provinces. Mountainous areas account for 94% of the total provincial area [45]. The region features high, medium, and low mountain ranges, hilly basins, deep valleys, and significant altitude differences (with altitude differentials exceeding 6600 m). Under the combined influence of these factors, Yunnan exhibits complex climate variability and frequent meteorological disasters [46]. The Ma-Zhao Expressway in Yunnan, located in the northeast, serves as a vital transportation artery connecting Yunnan to Sichuan Province and the mainland, playing a significant role in the economic development of the surrounding areas. However, due to its location along the main path of cold air invasion into Yunnan and its high altitude, the northeast of Yunnan experiences frequent dense fog events, which significantly impact the safe operation of the Ma-Zhao Expressway. Previous studies have shown that there is limited research on dense fog in Yunnan, especially focusing on the characteristics and formation mechanisms of dense fog on high-altitude mountainous expressways in Yunnan. As the relationship between fog and meteorological factors varies greatly under different conditions, the characteristics and formation mechanisms of dense fog on high-altitude mountainous expressways in Yunnan are unclear.

In late autumn 2022, from 24 to 30 October, consecutive dense fog events occurred on the Ma-Zhao Expressway. Motivated by the need to better understand the characteristics and formation mechanisms of fog events on the Yunnan Expressway, this article examines the evolution characteristics, meteorological conditions, and circulation anomalies associated with consecutive dense fog events. We used the standardized anomaly method to conduct a synoptic circulation analysis. To quantitatively analyze the extreme physical parameters and circulation patterns, we effectively used one of the most common intuitive analytical methods for extreme forecasting and case research [47,48]. Chen et al. [2] also used this method to assess persistent events of dense fog over eastern China, which was linked to anomalous atmospheric circulation. Many previous fog studies have been based on conventional station observations available four times per day. This relatively low temporal resolution may restrict detailed analyses of the rapid evolution of visibility during

fog events. By contrast, the present study uses minute-resolution traffic meteorological data along the expressway, which allows a more continuous and refined depiction of fog variation and its associated meteorological conditions.

This study is structured as follows: Section 2 describes the data and analysis methods; Section 3 analyzes the evolution features, meteorological conditions, and associated circulation anomalies of the consecutive dense fog events; and Section 4 concludes the findings of this study.

## 2. Materials and Methods

### *2.1. Data*

The study focuses on the Ma-Zhao Expressway in northeastern Yunnan Province (Figure 1), where consecutive dense fog events occurred from 24 to 30 October 2022. Observation data were collected from 6 traffic meteorological observation stations (Bridge-Group Station, No.4 Self-Rescue-Ramp Station, Sanyu River Station, Shanggaoqiao Tunnel Station, Shachi Bridge Station, Hujiawan Tunnel Station) situated along the Ma-Zhao Expressway (Figure 1). Data is recorded every minute, and detailed information on the latitude, longitude, altitude, and observed variables for each station can be found in Table 1.

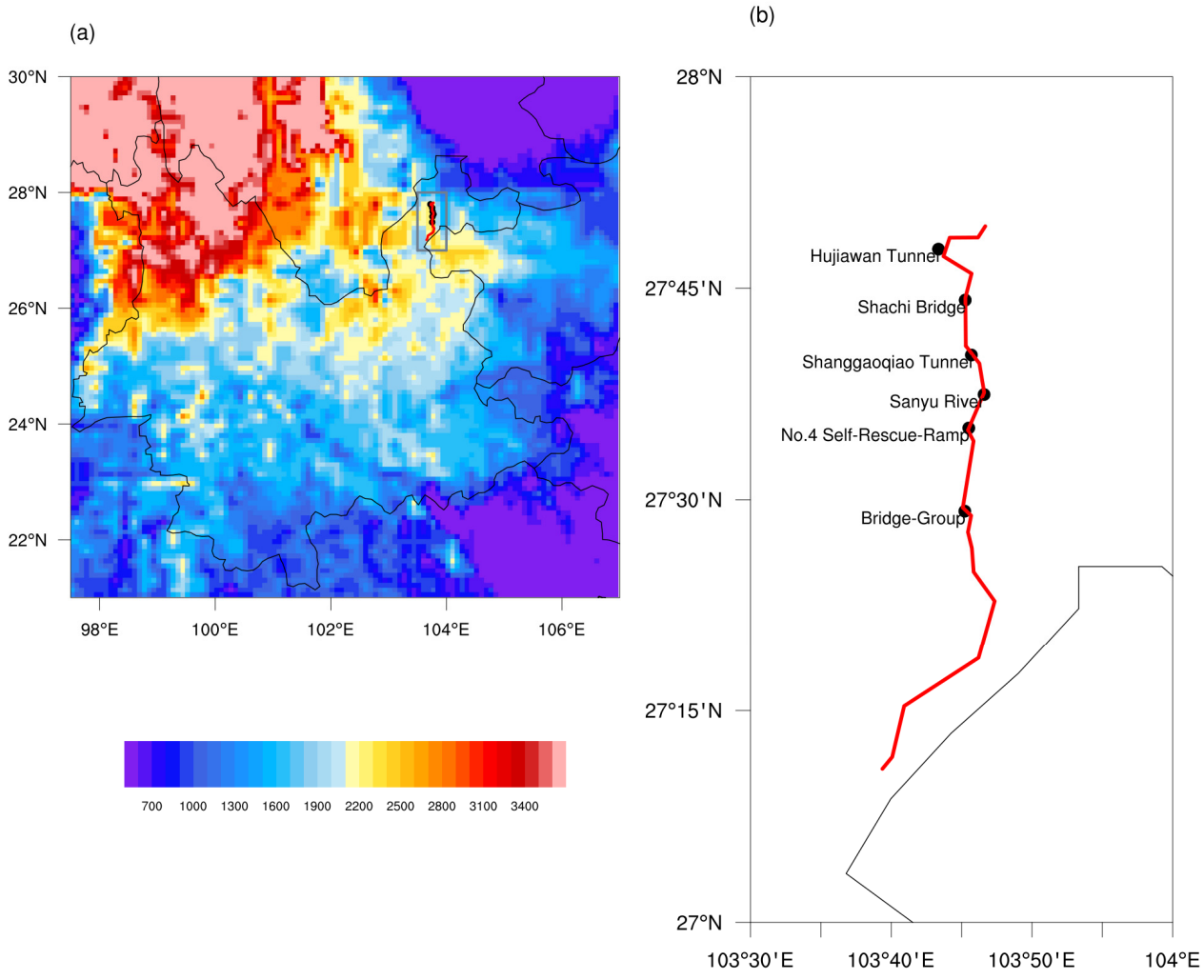


**Figure 1.** (**a**) The shaded area represents the altitude of Yunnan Province (units: m), with the grey box indicating the approximate range of the Ma-Zhao Expressway; (**b**) Enlarged view of the grey box area in (**a**), where the red line denotes the Ma-Zhao Expressway, and the black dots represent the locations of the traffic meteorological observation stations along the Ma-Zhao Expressway.

**Table 1.** The basic information of 6 traffic meteorological observation stations.

| Station Name | Longitude | Latitude | Altitude (m) | Observed Variables |
|---|---|---|---|---|
| Bridge-Group Station (BGS) | 103.7538 | 27.4865 | 1923 | visibility, air temperature, relative humidity, precipitation, wind speed |
| No.4 Self-Rescue-Ramp Station (N4SRRS) | 103.7585 | 27.5848 | 1760 | visibility, air temperature, relative humidity, precipitation |
| Sanyu River Station (SRS) | 103.7766 | 27.6244 | 1711 | visibility, air temperature, relative humidity, precipitation, wind speed |
| Shanggaoqiao Tunnel Station (STS) | 103.7616 | 27.6711 | 1620 | visibility, air temperature, relative humidity, precipitation |
| Shachi Bridge Station (SBS) | 103.7543 | 27.7360 | 1418 | visibility, air temperature, relative humidity, precipitation |
| Hujiawan Tunnel Station (HTS) | 103.7226 | 27.79622 | 1160 | visibility, air temperature, relative humidity, precipitation |

The hourly ERA5 reanalysis data (https://cds.climate.copernicus.eu/datasets, accessed on 2 April 2024) were utilized to analyze the meteorological conditions and circulation patterns of the consecutive dense fog events. The reanalyzed variables include air temperature, horizontal winds, geopotential height, specific humidity, relative humidity at 8 standard pressure levels ranging from 800 to 500 hPa, as well as 10 m winds, skin temperature, 2 m temperature, 2 m dewpoint, vertical integral of water vapor flux, and its divergence at a single level, with a horizontal resolution of 0.25 × 0.25. All times in this study are presented in local time (UTC+8).

Detailed definitions of the ERA5 reanalysis variables used in this study are consistent with the official dataset documentation:

Air temperature: Temperature of air at 800–500 hPa pressure levels, measured in kelvin (K); it is convertible to degrees Celsius (°C) by subtracting 273.15. It reflects the thermal state of the atmosphere at corresponding vertical levels.

Horizontal winds: Zonal (u) and meridional (v) components at 800–500 hPa pressure levels and 10 m above the surface, with units of m $s^{-1}$. The 10 m wind components represent near-surface horizontal air movement (eastward for u-component, and northward for v-component), and their combination determines wind speed and direction. Note that model-derived wind data averages local terrain, vegetation, and building effects, which may differ from site-specific observations.

Geopotential height (GH): The height of atmospheric pressure levels (800–500 hPa) in geopotential metres (gpm), used to characterize large-scale circulation patterns.

Specific humidity (SH): The mass of water vapor per unit mass of dry air (units: g $kg^{-1}$), representing the absolute moisture content of the atmosphere.

Relative humidity (RH): The ratio of actual water vapor pressure to saturated water vapor pressure at the same temperature (expressed as %), indicating the degree of air saturation.

The 2 m dewpoint temperature: The temperature to which air at 2 m above the surface must be cooled to reach saturation (units: K), a key indicator of air humidity. It is calculated by interpolating between the lowest model level and the surface, accounting for atmospheric conditions, and is convertible to °C by subtracting 273.15.

The 2 m temperature: The temperature of air at 2 m above land, sea, or inland waters (units: K), calculated via interpolation between the lowest model level and the surface. This is convertible to °C by subtracting 273.15.

Vertical integral of water vapor flux and its divergence: Water vapor flux quantifies the intensity of horizontal water vapor transport (units: kg $m^{-1}$ $s^{-1}$). Its divergence (units: kg $m^{-2}$ $s^{-1}$) indicates regional water vapor convergence (negative values) or divergence (positive values); negative divergence denotes the study area as a water vapor sink.

Skin temperature: The temperature of the Earth's surface (land, sea, or inland waters, units: K), reflecting the surface thermal state.

Surface pressure: Atmospheric pressure on the Earth's surface (units: Pa), representing the weight of the air column above a fixed point. It is often used with temperature to calculate air density, and 1 hPa = 1 mb = 100 Pa.

### *2.2. Methods*

To explore how meteorological factors influence visibility changes, we computed the correlation coefficients between various meteorological conditions and hourly visibility. The correlation analysis spanned 175 h, from 12 o'clock on 24 October to 18 o'clock on 31 October 2022.

Traditional pressure-level circulation fields often fall short in determining whether a weather event significantly deviates from the norm due to year-round and regional variabilities. To objectively evaluate the relative rarity of events, we proposed a normalized departure from local climatology [47]. To pinpoint the meteorological conditions advantageous to rare consecutive events of dense fog in late autumn 2022 along the Ma-Zhao Expressway, we determined the standard anomalies and original values of the daily mean circulation fields. The standardized anomaly (SA) was calculated following the methodology in previous studies [49], with the formula:

$$SA = (V - M)/\sigma, \quad (1)$$

where V is the variable value at a specific location or moment; σ and M are the standard deviation and climate mean of that variable at the same place and time, respectively. The SA value is the multiple of the variable's anomaly relative to the climate standard deviation σ. In the case of $|SA| \geq 3$, a more significant anomaly is indicated. We used samples from 21 days (10 days before and after the current day) to calculate the 30-year climate standard deviation and mean from 1992 to 2021. We used the hourly ERA5 reanalysis data as the basis for climate analysis. The analysis covered the period from 24 to 30 October over a 7-day timeframe. To determine the significance of the standardized anomaly and correlation coefficient, we applied Student's *t*-test.

Due to the possibility of rapid visibility reduction caused by intense short-term rainfall, we examined the cumulative precipitation during each of the seven low visibility events that occurred on the Ma-Zhao Expressway from 24 to 30 October 2022. We specifically focused on the cumulative precipitation amounts recorded at all stations during the periods when visibility dropped below 500 m. The cumulative rainfall amounts for each of these low visibility events were as follows: 4 mm, 0 mm, 1.5 mm, 2.6 mm, 0.8 mm, 0.8 mm, and 4.2 mm. Additionally, the relative humidity at all stations remained above 95% when visibility was below 500 m. Based on these observations and considering the definition of fog in previous research [2,15,40], it is reasonable to attribute these seven low visibility events to seven dense fog events.

## 3. Results

### *3.1. The Evolution of the Consecutive Dense Fog Events*

From 24 to 30 October 2022, the Ma-Zhao Expressway experienced seven consecutive dense fog events with strong intensity and long duration. Figure 2 illustrates the temporal

variation characteristics of visibility observed by 6 traffic meteorological observation stations located along the expressway: Bridge-Group Station, No.4 Self-Rescue-Ramp Station, Sanyu River Station, Shanggaoqiao Tunnel Station, Shachi Bridge Station, and Hujiawan Tunnel Station.

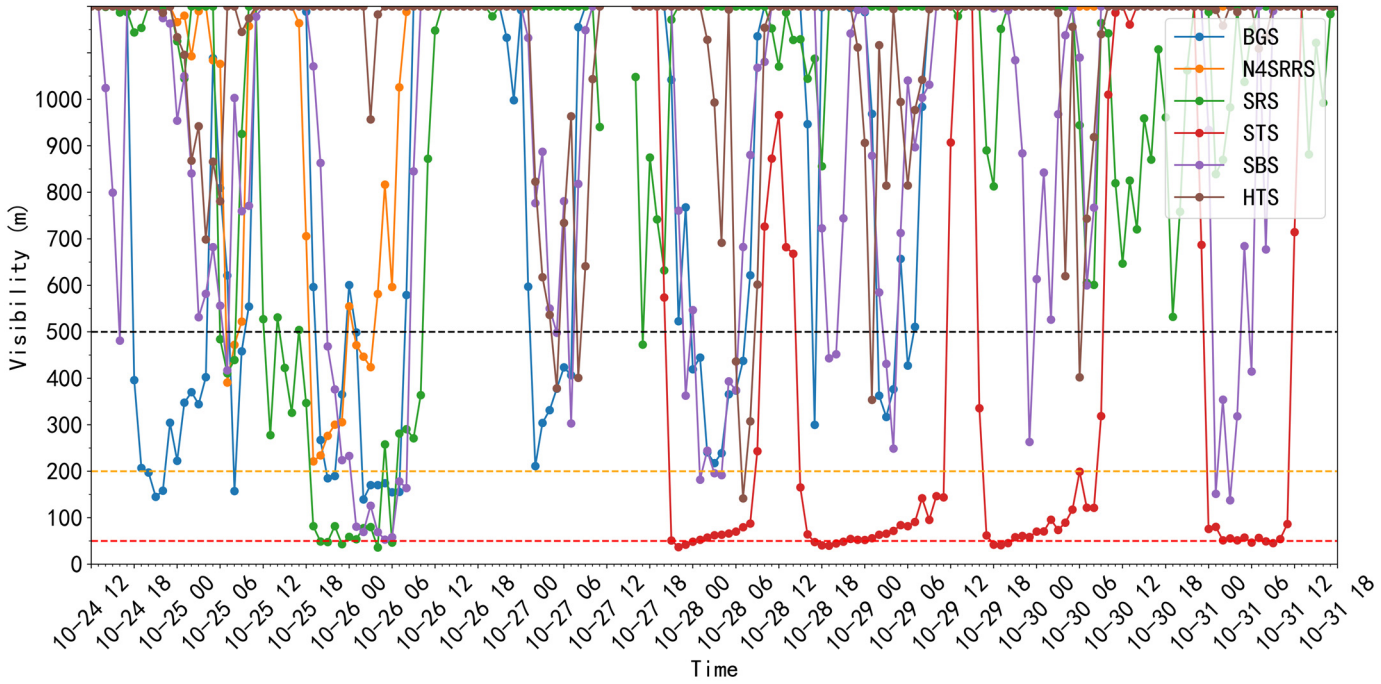


**Figure 2.** The temporal variations in visibility (units: m) observed by 6 traffic meteorological observation stations located along the Ma-Zhao expressway from 12:00 on 24 October to 18:00 on 31 October. (For the convenience of observing the variation characteristics of visibility during low visibility conditions, variations in visibility above 1200 m were omitted, the red, yellow and black dashed lines represents the visibility threshold of 50, 200 and 500 m, respectively).

At 18:00 on 24 October 2022, visibility at the Bridge-Group Station was initially reduced to less than 500 m. Subsequently, the dense fog event gradually spread to the surrounding stations, and the intensity was strengthened. By 20:00 on 24 October, the visibility at the Bridge-Group Station dropped to less than 200 m. Between 06:00 and 07:00 on 25 October, the visibility at Sanyu River Station, Shachi Bridge Station, and No.4 Self-Rescue-Ramp Station also decreased below 500 m. However, by 10:00 on the morning of 25 October, the visibility at these four stations had improved to more than 500 m, and the fog gradually dissipated. The Bridge-Group Station primarily observed this fog process, with a minimum visibility of less than 200 m. The fog event began around 18:00 on 24 October and dissipated by 10:00 on the morning of 25 October, lasting approximately 16 h.

Two hours later, by 12:00 on 25 October, the visibility at the Sanyu River station once again dropped to below 500 m. It remained in the range of 200–500 m until 18:00 on the 25th. Subsequently, the intensity of the dense fog noticeably increased, and its coverage expanded further to nearby stations. By 19:00 on the 25th, the visibility at the Sanyu River station decreased to approximately 50 m, and it remained at around 50 m until 06:00 on the 26th, with the lowest visibility during this period being less than 50 m. At the same time, the visibility at the No.4 Self-Rescue-Ramp station, Bridge-Group station, and Shachi Bridge station dropped below 500 m at 19:00, 20:00, and 21:00 on the 25th, respectively. By 01:00 and 02:00 on the 26th, the visibility at the Shachi Bridge and Bridge-Group stations decreased to below 200 m, and it remained in the range of 50–200 m until 07:00 on the 26th. By 08:00, 09:00, and 11:00 on the 26th, the visibility at the Bridge-Group, Shachi Bridge, and Sanyu River stations successively improved to above 500 m, and the dense fog gradually

dissipated. This dense fog event was most pronounced at the Sanyu River station, starting from 12:00 on the 25th, dissipating at 11:00 the following day, lasting approximately 23 h.

The intensity of the third dense fog event was relatively weaker, and its duration was relatively shorter. At 02:00 on 27 October, the visibility at the Bridge-Group station dropped to around 200 m. Subsequently, the visibility remained within the range of 200–500 m, and by 08:00, it rose to above 500 m. The visibility at Hujiawan Tunnel station and Shachi Bridge station also decreased to below 500 m at 04:00 on the 27th. Later, at the Hujiawan Tunnel station, the visibility fluctuated to around 600 m and 800 m between 06:00 and 07:00, and then dropped to around 300 m, stabilizing above 500 m by 09:00. Similarly, the visibility at the Shachi Bridge station rose to 600 m at 06:00, and then dropped to around 300 m, stabilizing above 500 m by 08:00.

At 20:00 on 27 October, the visibility at the Shanggaoqiao Tunnel station dropped to around 500 m. By 21:00, the visibility rapidly decreased to approximately 50 m and remained at this level. During this period, the lowest visibility was less than 50 m, which persisted until 09:00 on the 28th when the visibility began to improve, reaching above 500 m by 10:00 on the 28th. The visibility at the Shachi Bridge station and Bridge-Group station also dropped below 500 m at 23:00 on the 27th and 00:00 on the 28th, respectively, and continued to decrease. Between 02:00 and 04:00 on the 28th, the visibility dropped to around 200 m and then rose to above 500 m by 07:00 on the 28th. The visibility at the Hujiawan Tunnel station briefly dropped below 500 m between 06:00 and 09:00 on the 28th.

The fifth dense fog event was observed at the Shanggaoqiao Tunnel Station around 14:00 on 28 October. From 14:00 to 16:00 on the 28th, the visibility at the station rapidly decreased from 600 m to around 50 m. From 17:00 to 21:00, the visibility was less than 50 m, and from that time until 11:00 on 29 October, the visibility remained in the range of 50–200 m. By 12:00 on the 29th, the visibility had risen to above 500 m. The Bridge Group Station, Shachi Bridge Station, and Hujiawan Tunnel Station also observed fluctuations in visibility, dropping below 500 m between 17:00 on 28 October and 08:00 on the 29th, but these periods of low visibility were not prolonged.

The sixth and seventh dense fog events were overall similar to the fifth, mainly observed at the Shanggaoqiao Tunnel Station. On 29 October at 16:00, the visibility at the Shanggaoqiao Tunnel Station dropped below 500 m, and by 17:00, it had rapidly decreased to around 50 m. From 18:00 to 20:00, the visibility was less than 50 m. From 21:00 to 08:00 on the 30th, the visibility remained in the range of 50–200 m, and then began to rise. By 10:00 on the morning of the 30th, the visibility had increased to above 500 m, and the dense fog gradually dissipated. However, by 00:00 on the 31st, the visibility once again dropped below 500 m, and it remained in the range of 50–100 m until 10:00 on the 31st. By 12:00, the visibility had risen to above 500 m, marking the end of the seven consecutive dense fog events.

We classified seven consecutive events of dense fog in October 2022 as abnormal climatic events along the Ma-Zhao Expressway in Yunnan Province. Two fundamental questions drove our research: What atmospheric conditions were advantageous to the development, formation, and duration of fog events? What unusual meteorological factors and circulation anomalies have had a significant impact on these successive events of dense fog? These pivotal inquiries serve as the foundation for our investigation into the meteorological factors and abnormal atmospheric circulations linked to this noteworthy weather phenomenon.

### *3.2. Meteorological Conditions During the Consecutive Dense Fog Events*

Numerous studies have demonstrated a strong correlation between the occurrence of fog and specific meteorological factors [8,50–52]. These meteorological conditions can

be broadly categorized into three main groups: dynamic, thermal, and vapor conditions, as outlined by Chen et al. [2]. These atmospheric factors evolved in a manner that was consistent with the hourly visibility we observed at the Shanggaoqiao Tunnel Station and Bridge-Group during the seven consecutive events of dense fog (see Figures 3 and 4 and Table 2). The findings underscore the significant impact of certain meteorological conditions on the formation, maintenance and dissipation of fog events.

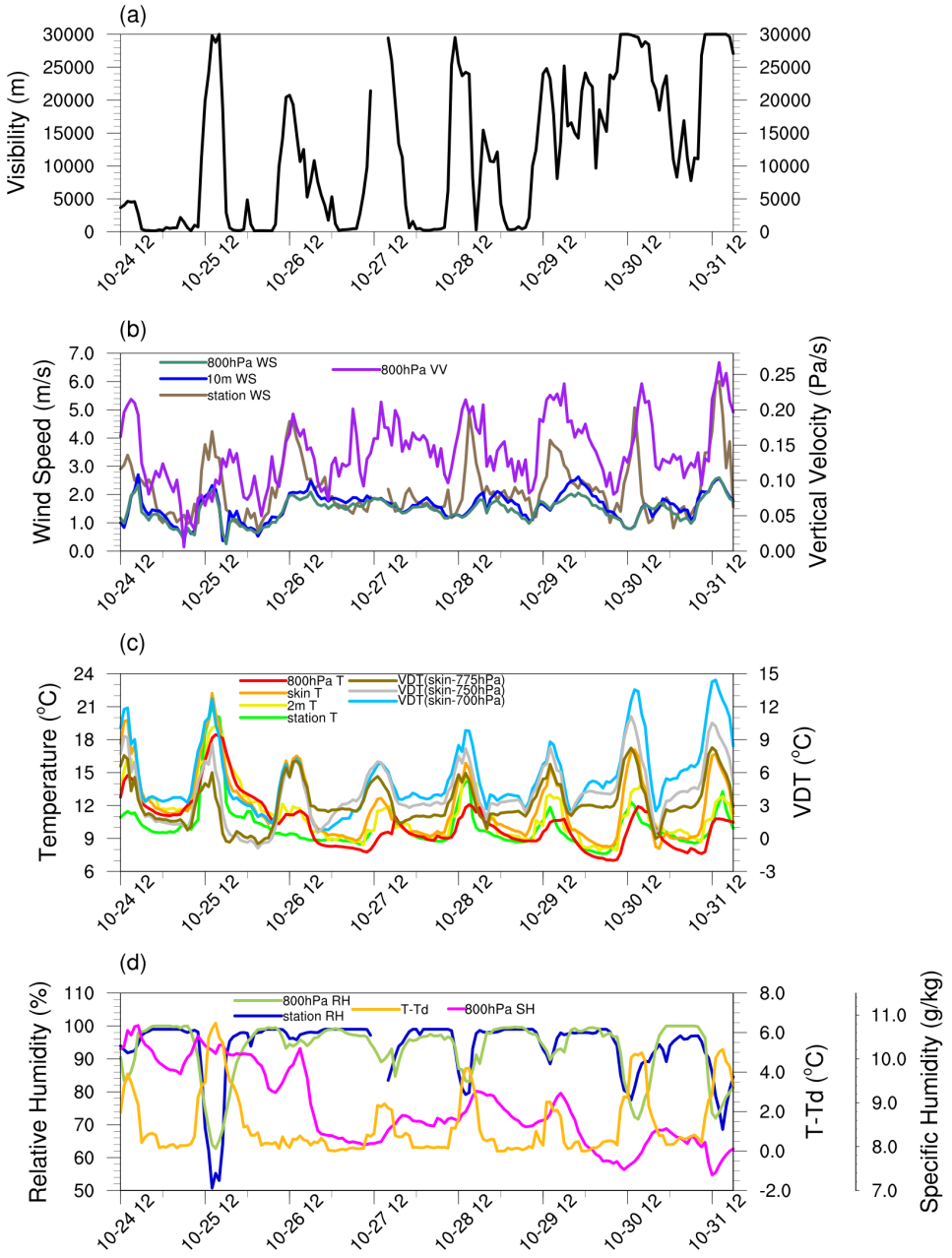


**Figure 3.** The hourly evolution of visibility and relevant meteorological factors at the Bridge-Group station from 12:00 on 24 October to 18:00 on 31 October: (**a**) visibility (units: m) observed by station; (**b**) wind Speed (WS, units: m/s) observed by station, 10 m and 800 hPa WS, 800 hPa Vertical Velocity (VV, units: Pa/s) from ERA5; (**c**) temperature (T, units: °C) observed at station, 2 m, skin surface and 800 hPa, vertical difference in temperature (VDT, units: °C) between skin surface and 700, 750 and 775 hPa from ERA5; (**d**) relative humidity (RH, unit: %) observed by station, 800 hPa RH and specific humidity (SH), 2 m dew point depression (difference between 2 m temperature and dew point temperature, T-Td, unit: °C) from ERA5.

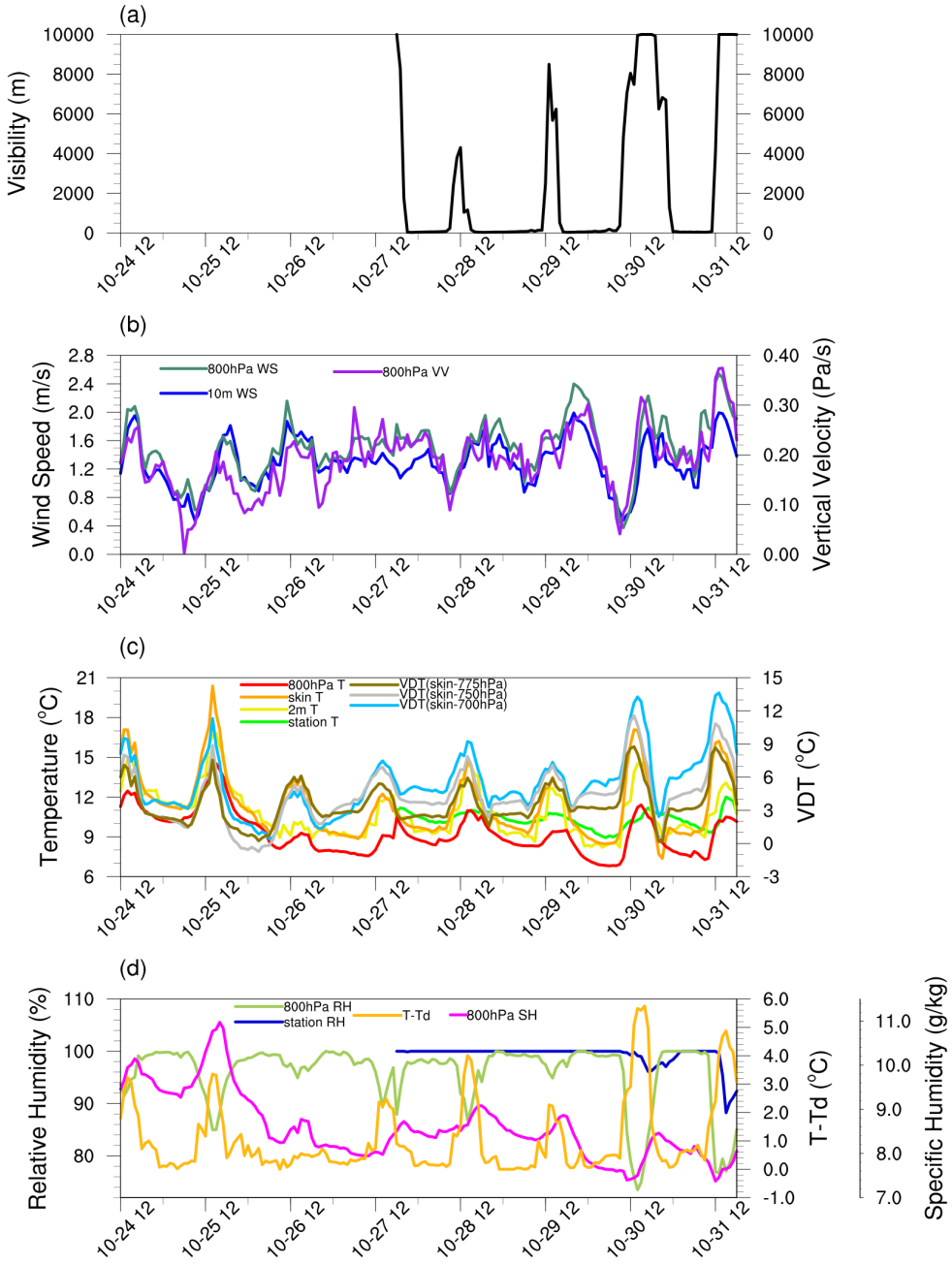


**Figure 4.** Same as Figure 3, but for the Shanggaoqiao Tunnel Station, the station observation data from 12:00 on 24 October to 17:00 on 27 October is missing.

**Table 2.** The summarization of the correlation coefficients of different meteorological factors with the hourly visibility variation at the Bridge-Group station and Shanggaoqiao Tunnel station from 12 o'clock on 24 October to 18 o'clock on 31 October 2022.

| Conditions | Factors | The Correlation Coefficient at the Bridge-Group Station | The Correlation Coefficient at the Shanggaoqiao Tunnel Station |
|---|---|---|---|
| Dynamical | Station Wind Speed | 0.47 ** | - |
| | 10 m Wind Speed | 0.27 ** | 0.12 |
| | 800 hPa Wind Speed | 0.39 ** | 0.21 |
| | 800 hPa Vertical Velocity | 0.42 ** | 0.38 ** |

**Table 2.** *Cont.*

| Conditions | Factors | The Correlation Coefficient at the Bridge-Group Station | The Correlation Coefficient at the Shanggaoqiao Tunnel Station |
|---|---|---|---|
| Thermal | Station Air Temperature | 0.35 ** | 0.49 ** |
| | 2 m Temperature | 0.14 | 0.58 ** |
| | Skin Temperature | 0.33 ** | 0.60 ** |
| | 800 hPa Temperature | 0.02 | 0.59 ** |
| | Vertical difference in temperature (VDT) between skin surface and 700 hPa | 0.67 ** | 0.58 ** |
| | VDT between skin surface and 750 hPa | 0.68 ** | 0.52 ** |
| | VDT between skin surface and 775 hPa | 0.60 ** | 0.49 ** |
| Vapor | Station Relative Humidity | −0.63 ** | −0.63 ** |
| | 800 hPa Relative Humidity | −0.56 ** | −0.78 ** |
| | 800 hPa Specific Humidity | −0.45 ** | −0.32 * |
| | 2 m Dew Point depression | 0.52 ** | 0.72 ** |

** denotes correlation coefficients significant at the 99% confidence level. * denotes correlation coefficients significant at the 95% confidence level.

#### 3.2.1. Dynamical Conditions

From a dynamic perspective, fogs are unlikely to form in conditions characterized by strong surface winds or intense vertical motions. Figure 3a,b illustrate the hourly variations from 24 October, 12:00, to 31 October, 18:00, for visibility at the Bridge-Group Station alongside the observed wind speeds at the station, 10m wind speeds, 800 hPa wind speeds, and 800 hPa vertical velocities from ERA5 reanalysis data at the grid point corresponding to the Bridge-Group Station location. The relationship between visibility and wind speed is evident, with visibility decreasing as wind speed decreases, and vice versa. The correlation coefficients between the visibility series and station wind speed, 10 m wind speed, and 800 hPa wind speed are 0.47, 0.27, and 0.39 (Table 2), respectively, passing significance tests at the 99% confidence level, indicating a strong positive correlation between visibility and wind speed. Regarding vertical velocity, the decrease in visibility aligns with a reduction in the absolute value of vertical velocity, signifying a weakening of vertical motion. Conversely, an increase in visibility corresponds to an increase in the absolute value of vertical velocity, with a correlation coefficient of 0.42 (Table 2) passing a significance test at the 99% confidence level, demonstrating a clear positive correlation. The changes in visibility and wind speed, as well as vertical velocity, at Shanggaoqiao Tunnel Station from 24 October, 12:00, to 31 October, 18:00, as shown in Figure 4a,b, exhibit similar overall characteristics to those observed at the Bridge-Group Station. It should be noted that observation data at Shanggaoqiao Tunnel Station are missing from 24 October, 12:00, to 27 October, 17:00, and the station lacks a wind speed observation sensor, resulting in no wind speed data. Nevertheless, the analysis suggests that lower (higher) surface wind speeds and weaker (stronger) vertical motions are associated with lower (higher) visibility. Our results revealed that limited diffusion of air or mixing in the lower troposphere was favorable to fog droplet accumulation and limited surface visibility. A static and stable atmosphere was most conducive to fog concentration and formation.

#### 3.2.2. Thermal Conditions

The unique thermal conditions that influence the evolution of visibility are of significant interest. Figure 3c displays the hourly variations from 24 October, 12:00, to 31 October, 18:00, of temperature-related data at the Bridge-Group Station, including station temperature, 2 m temperature, skin temperature, 800 hPa temperature, and vertical difference in temperature (VDT) between the skin surface and various layers (700 hPa, 750 hPa, 775 hPa) from ERA5 reanalysis data at the grid point corresponding to the Bridge-Group Station location. Decreases in temperature lead to a reduction in saturated water vapor pressure, facilitating moisture saturation and condensation. The graph illustrates that dips in visibility often align with dips in near-surface temperatures (station temperature, 2 m temperature, skin temperature, 800 hPa temperature), while increases in visibility correspond to rises in near-surface temperatures. Therefore, there is a positive correlation between visibility changes and near-surface temperature variations, with correlation coefficients of 0.35 and 0.33 for station temperature and skin temperature (Table 2), respectively, passing significance tests at the 99% confidence level, although the coefficients are lower for 2 m temperature and 800 hPa temperature. Furthermore, previous studies have shown that atmospheric temperature inversion layers play a crucial role in the occurrence and maintenance of dense fog. The changes in VDT between the skin surface and lower troposphere (700, 750, 775 hPa) reveal that periods of low visibility often coincide with minimal VDT, indicating a reduced temperature contrast between surface and lower troposphere, or even negative differentials, signifying the presence of atmospheric temperature inversion conditions. The correlation coefficients between visibility changes and VDT between surface and different layers (700, 750, 775 hPa) are 0.67, 0.68, and 0.60 (Table 2), respectively, passing significance tests at the 99% confidence level. The corresponding relationship between visibility, air temperature, and VDT between the skin surface and lower troposphere at Shanggaoqiao Tunnel Station also exhibits similar characteristics to those of the Bridge-Group Station (Figure 4a,c). This suggests that a stronger and prolonged temperature inversion favors reduced visibility, leading to the persistence of heavy fog. We connected this inversion structural formation to localized surface cooling and warm advection in the lower layer of the troposphere.

#### 3.2.3. Vapor Conditions

Numerous small droplets of water create fog. A saturated vapor environment is necessary for fog to form and persist, which demonstrates the essential role of relative and absolute humidity in fog events. Figure 3d illustrates the hourly variations from 24 October, 12:00, to 31 October, 18:00, of station and 800 hPa relative humidity, 800 hPa specific humidity, and the 2 m dew point depression (the difference between the temperature and dew point temperature at 2 m). The graph reveals that during periods of low visibility, relative humidity levels are consistently close to 100%, and the 2 m dew point depression approaches zero degrees, indicating near-saturation of water vapor. The correlation coefficients between the visibility change series and station relative humidity, 800 hPa relative humidity, and 2 m dew point depression are −0.63, −0.56, and 0.52 (Table 2), respectively, passing significance tests at the 99% confidence level. However, the peak specific humidity moments do not align with periods of reduced visibility but occur before visibility decreases. This suggests that specific humidity notably increases before the onset of dense fog, leading to a significant drop in visibility. The correlation coefficient between specific humidity and visibility is −0.45 (Table 2), also passing a significance test at the 99% confidence level. Similar characteristics are also observed at Shanggaoqiao Tunnel Station (Figure 4d). The strong correlations observed between humidity factors (such as 800 hPa relative humidity, 2 m dew point depression and 800 hPa specific humidity) and visibility indicate that higher

vapor content and increased saturation near the surface promote water vapor condensation, thereby contributing to the formation or intensification of fog phenomena.

Our analysis verified that specific atmospheric conditions in late autumn 2022 well-configured these seven consecutive events of dense fog along the Ma-Zhao Expressway. These conditions included an inverted temperature structure, saturated surface air, and weak dynamic progress. Therefore, the subsequent research in this paper will further investigate how the large-scale background circulation anomalies play a crucial role in shaping such meteorological conditions.

### *3.3. The Large-Scale Anomalies Associated with the Consecutive Dense Fog Events*

Utilizing the widely employed standardized anomaly method outlined in Section 2.2, a detailed analysis of the circulation and physical quantity anomalies during the seven consecutive dense fog events was conducted. The analysis of the standardized anomalies was performed on all fields for foggy days from 24 to 30 October 2022.

#### 3.3.1. Circulation Anomalies

Figure 5 depicts the distributions of the original, climatic, and anomalous geopotential heights (GH) at 500 and 700 hPa levels during the seven consecutive dense fog days. From Figure 5a, it is evident that the control range of the western Pacific subtropical high (WPSH) at 500 hPa significantly expanded westward, covering most of the regions from southern Yunnan to the central–southern Indochina Peninsula. The northeastern part of Yunnan, where the consecutive fog events occurred, was under the influence of a weak geopotential height ridge line. The 500 hPa geopotential heights exhibited significant positive anomalies (exceeding 2 standard deviations) over continental regions from Yunnan Province to northeastern China, while negative anomalies were observed in the Philippines to southeastern Japan, with the center of the negative anomaly located over the Philippines (Figure 5e). The distribution pattern of the 700 hPa geopotential height anomalies (Figure 5f) was similar to that of the 500 hPa level. However, the positive anomalies in the northeastern part of China were more pronounced, and the range of negative geopotential height anomalies (exceeding 2 standard deviations) in the Philippines region was larger (Figure 5f).

The distributions of the original, climatic, and anomalous wind fields at 500 and 700 hPa levels are shown in Figure 6. At the 500 hPa level during the period of consecutive dense fog, the anticyclonic circulation over the northwestern part of the South China Sea exhibited a more westward and northward bias in its center compared to the climatological state, with a stronger intensity of the anticyclone (Figure 6a,c). Looking at the anomaly fields, in accordance with the theory of geostrophic wind equilibrium, corresponding to the widespread positive anomalies in geopotential heights from Yunnan to northeastern China, an anomalous anticyclonic circulation pattern was observed over the same region, while a cyclonic circulation anomaly was present in the Philippines region (Figure 6e). The anomalous characteristics of the 700 hPa wind field were generally similar to those at 500 hPa, but the cyclonic circulation anomaly in the Philippines region was more pronounced, and a significant southerly wind anomaly was observed in the northeastern part of Yunnan (Figure 6f). The southerly wind anomaly in northeastern Yunnan may have provided favorable conditions for the occurrence of the consecutive dense fog events by influencing local temperature changes and moisture transport. Therefore, the next step will involve analyzing the anomalous characteristics of the temperature and humidity fields in detail.

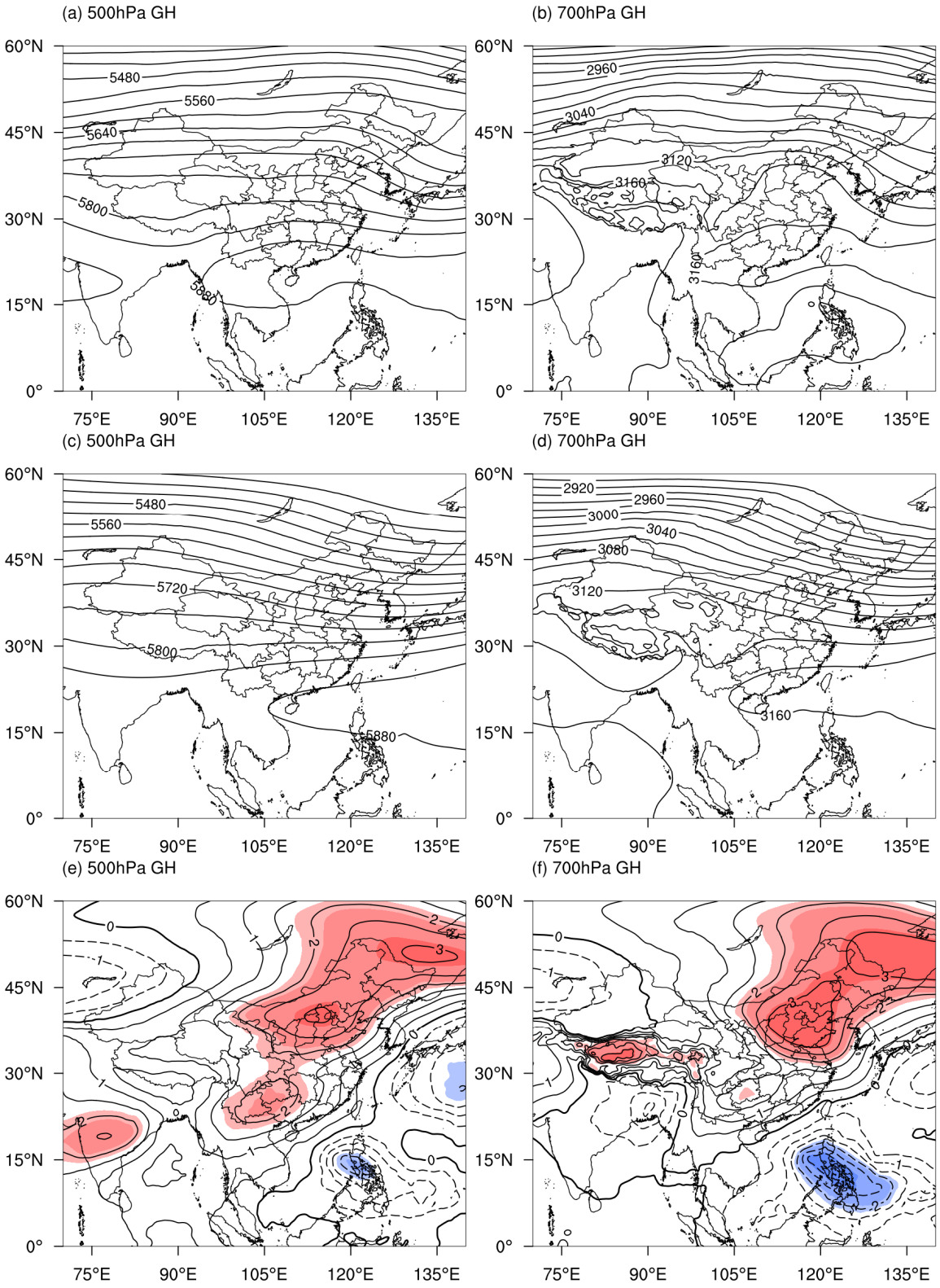


**Figure 5.** The original ((**a**,**b**), units: gpm) and standardized anomalies (**e**,**f**) of geopotential heights (GH) at 500 (**a**,**e**) and 700 (**b**,**f**) hPa levels averaged from 24 to 30 October 2022. The 30-year climate mean (units: gpm) of GH at 500 (**c**) and 700 (**d**) hPa levels averaged from 24 to 30 October after a 21-day binomial filter. Contour intervals are 40 gpm in (**a**,**c**), 20 gpm in (**b**,**d**) and 0.5 standard deviations in (**e**,**f**). In (**e**,**f**), solid lines mark the positive values, and dashed lines mark the negative values; the bold line denotes zero. Areas shaded in (**e**,**f**) from light to dark denote the standardized anomalies passing the significance test at 90, 95 and 99% confidence level, respectively.

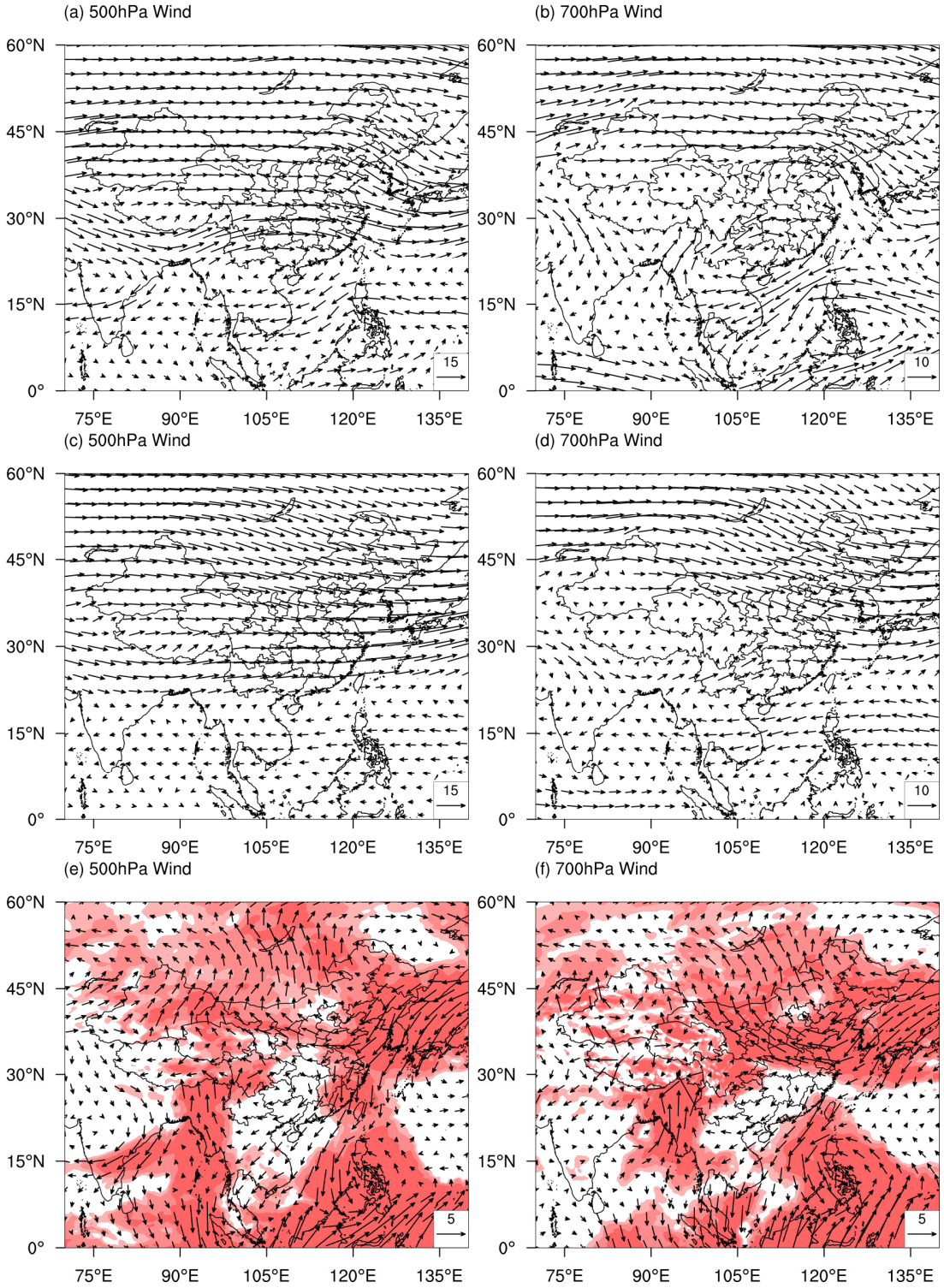


**Figure 6.** The original ((**a**,**b**), units: m/s) and standardized anomalies (**e**,**f**) of horizontal winds at 500 (**a**,**e**) and 700 (**b**,**f**) hPa levels averaged from 24 to 30 October 2022. The 30-year climate mean (units: m/s) of winds at 500 (**c**) and 700 (**d**) hPa levels averaged from 24 to 30 October after a 21-day binomial filter. Areas shaded in (**e**,**f**) from light to dark denote the standardized anomalies passing the significance test at 90, 95 and 99% confidence level, respectively.

### 3.3.2. Temperature Anomalies

The profiles of the vertical distributions of the original, climatic, and anomalous air temperatures at the Bridge-Group Station are illustrated in Figure 7. From the figure, it is evident that the average air temperatures in the lower to middle troposphere at the

Bridge-Group Station from 24 to 30 October 2022 were significantly higher than the climatological temperatures for the same period (Figure 7a). Positive temperature anomalies were observed from 800 hPa to 500 hPa, with the peak of the positive anomaly occurring near 700 hPa, reaching a value of 1.7 standard deviation anomalies (Figure 7b). This is conducive to the formation of a temperature inversion layer in the lower troposphere. The lower tropospheric anomalous inversion enhanced the near-surface atmosphere stability, which supported the ability of fog to form and persist. We examined the original 700 hPa winds and air temperature averages between 24 and 30 October 2022 (Figure 8). We attributed the notably warm temperature anomalies to the southerly flows over northeastern Yunnan. The northward wind was nearly perpendicular to the isotherm in this province.

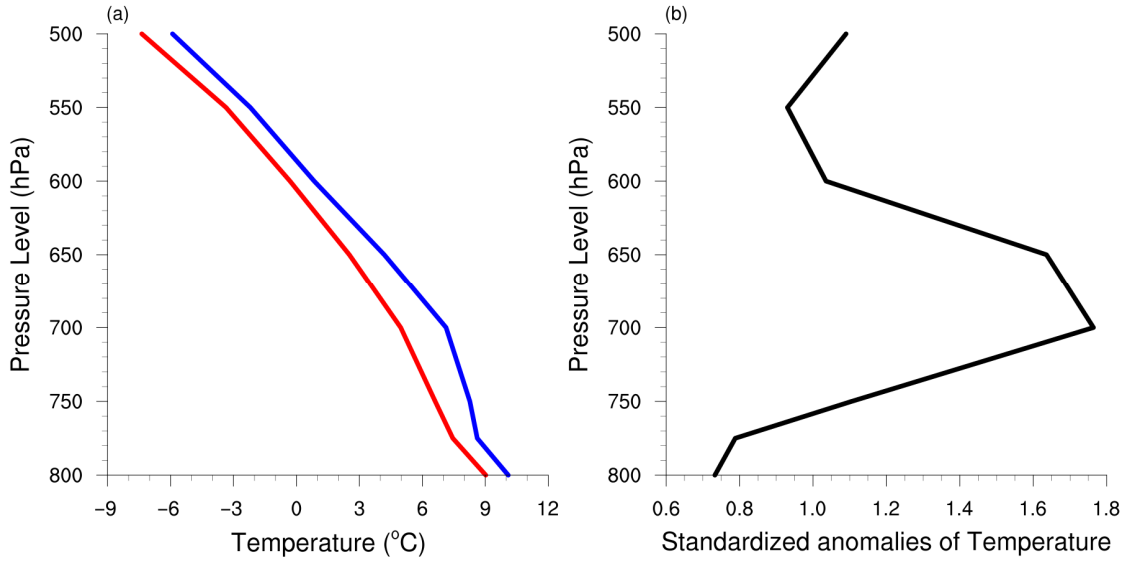


**Figure 7.** The profiles of original (blue line in (**a**), units: °C) and standardized anomalies (**b**) of air temperature at the Bridge-Group Station averaged from 24 to 30 October 2022. The profiles of the 30-year climate mean (red line in (**a**), units: °C) of air temperature at the Bridge-Group Station averaged from 24 to 30 October after a 21-day binomial filter.

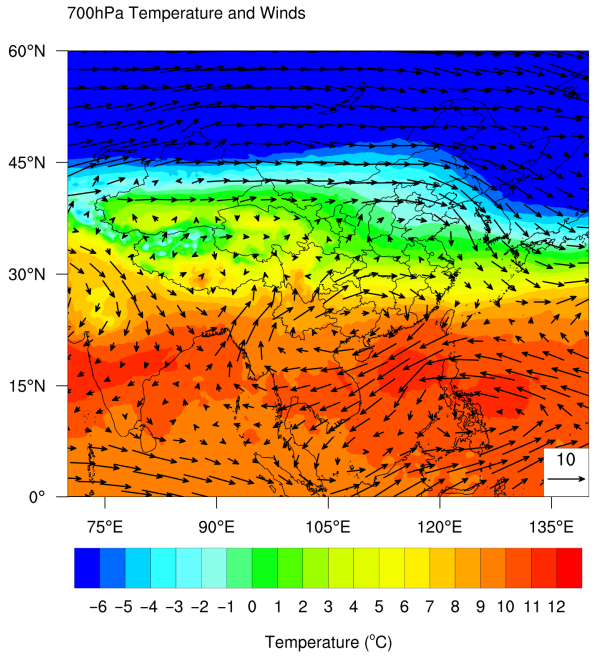


**Figure 8.** The original horizontal winds (vectors, units: m/s) and air temperature (shade, units: °C) at the 700 hPa level averaged from 24 to 30 October 2022.

### 3.3.3. Water Vapor Anomalies

Adequate water vapor supply is essential for the occurrence of dense fog events. The water vapor characteristics during the period of consecutive dense fog events are analyzed based on the standardized anomalies of column-integrated water vapor flux (CIWVF) and its divergence, specific humidity, and relative humidity. Figure 9 illustrates the distributions of the standardized anomalies of CIWVF and its divergence. From the figure, a distinct anomalous water vapor transport path can be observed, originating from the East China Sea region, moving from north to south, then turning from east to west at the northeastern corner of the Indochina Peninsula, and finally shifting from south to north in southern Yunnan (Figure 9a), thereby enhancing the water vapor transport to northeastern Yunnan. The standardized CIWVF anomaly value at northeastern Yunnan is approximately 2 standard deviations. Additionally, examining the standardized anomaly of CIWVF divergence reveals a significant negative divergence anomaly at northeastern Yunnan (Figure 9b), passing a significance test at the 99% confidence level, indicating northeastern Yunnan acts as a water vapor sink, where a substantial amount of water vapor is transported and converged. The profiles of the original, climatic, and anomalous specific humidity and relative humidity at the Bridge-Group Station are depicted in Figure 10. Consistent with the anomalous characteristics of the CIWVF and its divergence, positive anomalies in specific humidity prevail from the near-surface to the lower troposphere at the Bridge-Group Station. The peak of the specific humidity positive anomaly occurs near the 700 hPa level, reaching a value of 3 standard deviations (Figure 10b). Figure 10c illustrates that the average relative humidity from the near surface to the 650 hPa level at the Bridge-Group Station during the period of consecutive fog events was significantly higher than the climatological state for the same period, with standardized anomalies ranging from 1 to 2 standard deviations below the 700 hPa level (Figure 10d). This pattern aligns well with the positive specific humidity anomalies observed in this region. These positive anomalies in relative humidity create favorable conditions for water vapor condensation and the occurrence of dense fog events.

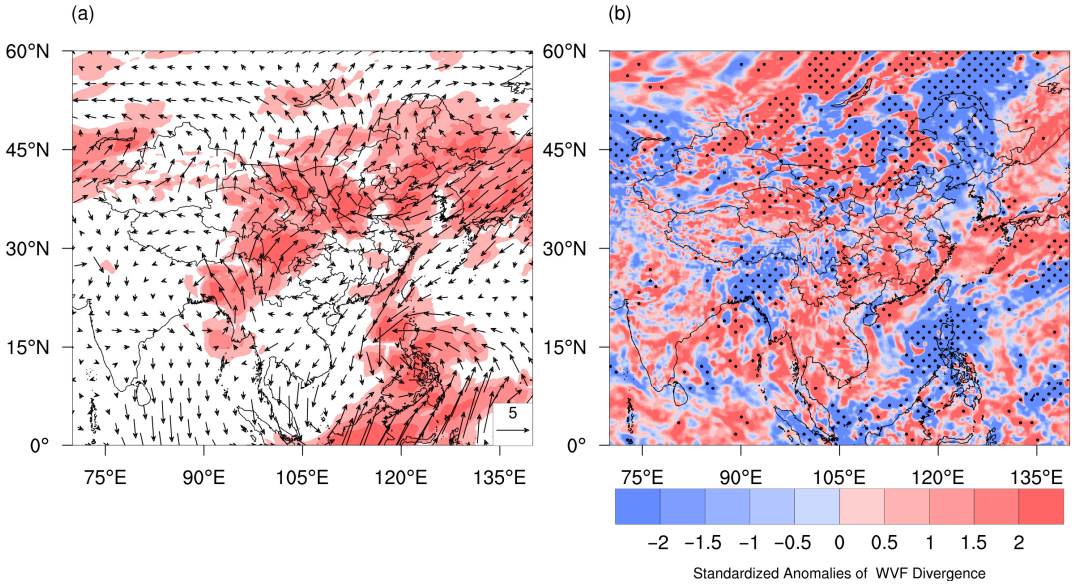


**Figure 9.** The standardized anomalies of column-integrated water vapor flux ((**a**), vectors) and its divergence ((**b**), shade) averaged from 24 to 30 October 2022. Areas shaded in (**a**) from light to dark denote the standardized anomalies passing the significance test at 90, 95 and 99% confidence level, respectively. Dotted areas in (**b**) represent the standardized anomalies passing the significance test at 99% confidence level.

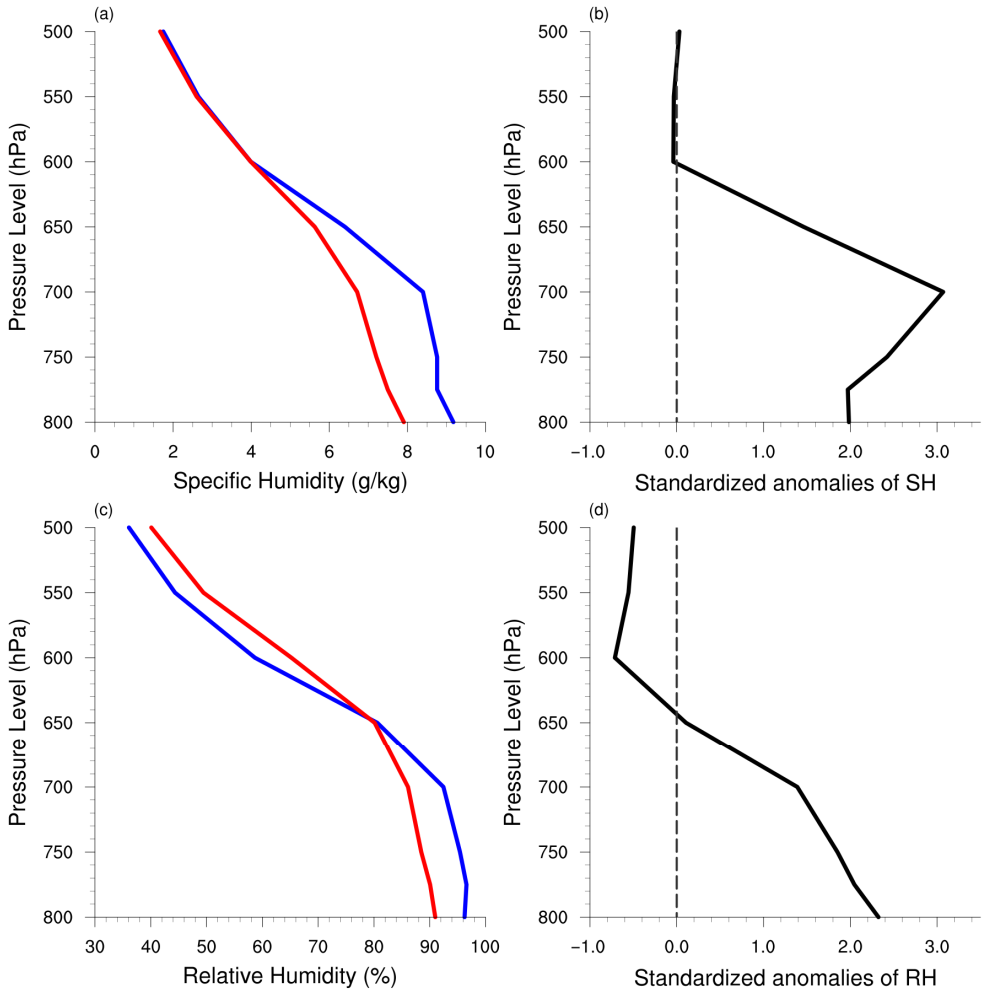


**Figure 10.** The profiles of original specific humidity (SH, blue line in (**a**), units: g/kg), standardized anomalies of SH (**b**), original relative humidity (RH, blue line in (**c**), units: %), standardized anomalies of RH (**d**) at the Bridge-Group Station averaged from 24 to 30 October 2022. The profiles of the 30-year climate mean of SH (red line in (**a**), units: g/kg) and RH (red line in (**c**), units: %) at the Bridge-Group Station averaged from 24 to 30 October after a 21-day binomial filter.

## 4. Discussion and Conclusions

Fog is a type of weather phenomenon characterized by low visibility near the surface, which can have adverse effects on traffic transportation. From 24 to 30 October 2022, the Ma-Zhao Expressway experienced seven consecutive episodes of dense fog. During these seven instances of dense fog, the cumulative duration of visibility below 500 m was approximately 110 h. The lowest visibility recorded during this period was less than 50 m. Additionally, these dense fog events exhibited characteristics of rapid visibility reduction. As a result, we identified the seven consecutive events of dense fog as significant unusual weather events with strong intensity and long duration.

Due to the significant impact of meteorological conditions on the occurrence and persistence of dense fog, this study analyzed the meteorological characteristics corresponding to the seven consecutive dense fog events. The analysis revealed a high correlation between hourly evolution of visibility and various meteorological factors during the period from 12:00 on 24 October to 18:00 on 31 October 2022. Advantageous atmospheric conditions for dense fog include an inverted lower layer in the troposphere, an abundant and saturated surface, and weak dynamic progress. For example, weaker vertical motion and wind speeds caused lower visibility to develop and persist. The periods of low visibility often coincide with minimal VDT between the skin surface and the lower troposphere, indicating

reduced temperature contrast or even negative differentials, which signifies the critical impact of temperature inversion conditions. Notably, we identified a significant correlation between specific humidity and visibility. Relative humidity and a 2 m dew point depression demonstrated that both relative and absolute humidity conditions were essential for these consecutive dense fog events with a strong intensity and long duration. These findings are consistent with many previous research results [2,51–53]. It is worth noting that in this study, the correlation coefficients between visibility and thermal and humidity factors were significantly higher than those between visibility and dynamic factors. This may indicate that for the consecutive dense fog events on the Ma-Zhao Expressway, the influence of thermal and moisture conditions is relatively more important than dynamic conditions, as emphasized in some previous studies regarding the importance of thermal and moisture conditions in the formation and persistence of fog [21,22].

We further assessed the unusual meteorological circulation pattern correlated with these consecutive events of dense fog. During the fog days, in the lower to middle troposphere, corresponding to the positive and negative anomalies in geopotential heights, an anomalous anticyclonic circulation pattern was observed from Yunnan to northeastern China, while a cyclonic circulation anomaly was present in the Philippines region. Within this atmospheric configuration, a significant southerly wind anomaly was observed in the northeastern part of Yunnan, where the consecutive dense fog events occurred. The notable southerly wind anomaly brought warm and moist air to the northeastern part of Yunnan. On one hand, this led to a significant warming in the lower troposphere (700–650 hPa), which favored the formation of temperature inversions. On the other hand, it brought abundant moisture, facilitating air saturation and ultimately creating favorable conditions for the occurrence, development, and persistence of the consecutive dense fog events. Similar findings can also be found in previous studies. According to Houssos et al. [53], the advection of humid and warm air masses with a weak southerly flow is a favorable meteorological condition in European fog events. Zhang et al. [51] demonstrated that anomalous southerly winds in the middle and lower troposphere are favorable for transporting more water vapor to eastern China, thereby promoting the maintenance and development of fog and haze in that region. According to Liu et al. [24], the upper-level warm advection and low-level cold advection significantly enhanced inversion intensity and promoted the development of fog. The vapor advection that resulted from the southerly winds caused the fog to intensify. Tian et al. [54] also discovered that the warm and moist southerly boundary layer low-level jet favors water vapor transport and the construction of inversion layers. The conclusions of this study align with the aforementioned findings from previous research.

In summary, the main conclusions of this study are as follows: Seven consecutive dense fog events with long durations and strong intensity occurred on the Ma-Zhao Expressway in northeastern Yunnan Province from 24 to 30 October 2022. Correlation analysis shows that thermal factors (the vertical temperature difference between skin surface and lower troposphere) and vapor factors (including specific humidity, 2 m dew point depression, and relative humidity) are significantly correlated with visibility, with correlation coefficients of 0.68 and −0.63, respectively, both significant at the 99% confidence level. These correlations are notably stronger than those of dynamic factors such as station wind speed ($r = 0.47$), highlighting the dominant roles of thermal and vapor conditions in the formation and maintenance of dense fog on the Ma-Zhao Expressway. In addition, the significant southerly wind anomaly in the lower troposphere, driven by the anomalous anticyclone east of Yunnan and the cyclone over the Philippines, acts as a key dynamic carrier. It transports warm air from low-latitude regions to facilitate inversion formation and conveys abundant moisture to the study area to support near-surface saturation. Standardized anomaly

analysis further reveals that this southerly wind anomaly and associated warm-moisture transport led to a positive temperature anomaly of 1.7 standard deviations near 700 hPa and a positive specific humidity anomaly of more than 2 standard deviations in the lower troposphere during the fog episodes. This dual effect of the southerly wind anomaly is consistent with the dominant influence of thermal and vapor factors identified in the correlation analysis, forming a consistent mechanism for the occurrence and enhancement of consecutive dense fog events. The results reveal key thermal and moisture conditions governing dense fog formation over the Yunnan low-latitude plateau. These findings have important practical implications for the forecasting and early warning of dense fog along mountain expressways to improve traffic safety and may also provide valuable references for fog prediction in analogous low-latitude plateau regions such as southern Sichuan, western Guizhou, and western Guangxi.

This study also has several limitations: simple correlation analysis has limitations in characterizing nonlinear atmospheric processes, and the traffic meteorological station data adopted has limited spatial representativeness; in addition, the key meteorological thresholds for fog formation and the relative importance of various influencing factors have not been quantitatively defined. For future work, we will introduce more advanced statistical methods and quantitative diagnostic indicators, clarify the critical meteorological thresholds, and further explore the formation mechanism of dense fog, so as to improve the accuracy of fog forecasting and early warning.

**Author Contributions:** Conceptualization, Y.D. and D.W.; methodology, Y.D.; software, Y.D.; validation, Y.D., D.W. and X.C.; data curation, X.Y. and C.X.; writing—original draft preparation, Y.D.; writing—review and editing, Y.D. and D.W.; visualization, Y.D.; supervision, D.W. All authors have read and agreed to the published version of the manuscript.

**Funding:** This research is jointly funded by the Yunnan Fundamental Research Project [grant numbers 202301AU070018, 202201AT070245, 202405AK340003]; Yunnan Research Project [grant number 202305AC160070]; and the Science and Technology Innovation Project of the Department of Transport of Yunnan Province [grant numbers YJKJB[2024]51, YJKJB[2024]52].

**Institutional Review Board Statement:** Not applicable.

**Informed Consent Statement:** Not applicable.

**Data Availability Statement:** The hourly ERA5 reanalysis data analyzed in this study comprises publicly available datasets. The data can be found here: https://cds.climate.copernicus.eu/datasets (accessed on 2 April 2024). Restrictions apply to the availability of the traffic meteorological station observation data. Data are available from the authors of this paper with the permission of Broadvision Engineering Consultants Co., Ltd.

**Acknowledgments:** We thank LetPub (www.letpub.com.cn) for its linguistic assistance during the preparation of this manuscript.

**Conflicts of Interest:** Authors Yuchao Ding, Xingtong Chen, Xuekun Yang and Chang'an Xiong are employed by the Broadvision Engineering Consultants Co., Ltd. The remaining author declares that the research was conducted in the absence of any commercial or financial relationships that could be construed as a potential conflict of interest.

## References

1. Gultepe, I.; Tardif, R.; Michaelides, S.; Cermak, J.; Bott, A.; Muller, M.; Pagowski, M.; Hansen, B.; Ellrod, G.; Jacobs, W.; et al. Fog Research: A Review of Past Achievements and Future Perspectives. *Pure Appl. Geophys.* **2007**, *164*, 1121–1159. [CrossRef]
2. Chen, S.; Liu, D.; Kang, Z.; Shi, Y.; Liu, M. Anomalous Atmospheric Circulation Associated with the Extremely Persistent Dense Fog Events over Eastern China in the Late Autumn of 2018. *Atmosphere* **2021**, *12*, 111. [CrossRef]

3. Zhang, Y.H.; Ou, B.; Sun, X.G. Analysis of Causes and Solutions for Highway Traffic Accidents in Heavy Fog Weather. *China Sci. Technol. Inf.* **2008**, *294*, 297. Available online: https://d.wanfangdata.com.cn/periodical/zgkjxx200819194 (accessed on 13 April 2026). (In Chinese)
4. Lee, Y.H.; Lee, J.; Park, S.K.; Chang, D.; Lee, H. Temporal and Spatial Characteristics of Fog Occurrence over the Korean Peninsula. *J. Geophys. Res.* **2010**, *115*, 2009JD012284. [CrossRef]
5. Shrestha, S.; Moore, G.A.; Peel, M.C. Trends in Winter Fog Events in the Terai Region of Nepal. *Agric. For. Meteorol.* **2018**, *259*, 118–130. [CrossRef]
6. Chen, X.X.; Guo, P.W.; Luo, Y. Climate Characteristics of Fog Days of Various Categories in China. *Clim. Change Res.* **2008**, *4*, 106–110. (In Chinese)
7. Wu, D.; Wu, X.J.; Li, F.; Tan, H.B.; Chen, J.; Chen, H.H.; Cao, Z.Q.; Sun, X. Long-term variation of fog and mist in 1951–2005 in mainland China. *J. Trop. Meteorol.* **2011**, *27*, 145–151. (In Chinese)
8. Ding, Y.H.; Liu, Y.J. Analysis of Long-Term Variations of Fog and Haze in China in Recent 50 Years and Their Relations with Atmospheric Humidity. *Sci. China Earth Sci.* **2014**, *57*, 36–46. (In Chinese) [CrossRef]
9. Lin, J.; Yang, G.M.; Mao, D.Y. Spatial and Temporal Characteristics of Fog in China and Associated Circulation Patterns. *Clim. Environ. Res.* **2011**, *13*, 171–181. Available online: https://wenku.baidu.com/view/a5d6b5bec77da26925c5b016?fr=xueshu&_wkts_=1776527017508 (accessed on 13 April 2026). (In Chinese)
10. Zheng, Y.P.; Li, J.L. A Study of the Climatic Characteristics of Heavy Fog In Urumqi in Recent 31 Years. *Meteorol. Mon.* **2008**, *34*, 22–28. (In Chinese) [CrossRef]
11. Fu, G.Q.; Zhang, Y.X.; Zhang, Q.H.; Zhang, N.; Zhang, Y.H. Analysis on Characteristics of Low Visibility Events in Hebei Province. *Meteorol. Mon.* **2013**, *39*, 1042–1049. (In Chinese) [CrossRef]
12. Gao, H.Y.; He, Y.; Wang, D.; Cai, X.L.; Yang, X. Temporal Variation and Cause Analysis of Fog Days in Xi'An City during Last 50 Years. *Plateau Meteorol.* **2013**, *32*, 1739–1746. (In Chinese) [CrossRef]
13. Chen, X.X.; Xu, A.H.; Xu, B.; Xiao, A. Characteristics of spatiotemporal distribution and influence elements of three kinds of regional heavy fog in Jiangxi province from 2000 to 2012. *J. Meteorol. Environ.* **2018**, *34*, 37–47. (In Chinese) [CrossRef]
14. Zong, C.; Qian, W.; Bao, Y.X.; Yuan, C.S.; Zhou, L.Y.; Cui, C.X.; Wang, H.B. Temporal-Spatial Variations of Summer Heavy Fog and Its Meteorological Influence Factors in Jiangsu Province. *Meteorol. Mon.* **2019**, *45*, 968–977. Available online: https://d.wanfangdata.com.cn/periodical/qx201907007 (accessed on 13 April 2026). (In Chinese)
15. Wang, H.B.; Zhang, Z.W.; Liu, D.Y.; Zu, F.; Zhu, Y.Y.; Wu, H. Characteristics of the Macro- and Micro-Structures of the Different Grades Fog in Jiangsu Province. *Plateau Meteorol.* **2021**, *40*, 1177–1188. (In Chinese) [CrossRef]
16. Nakanishi, M. Large-Eddy Simulation of Radiation Fog. *Bound.-Layer Meteorol.* **2000**, *94*, 461–493. [CrossRef]
17. Koračin, D.; Dorman, C.E.; Lewis, J.M.; Hudson, J.G.; Wilcox, E.M.; Torregrosa, A. Marine Fog: A Review. *Atmos. Res.* **2014**, *143*, 142–175. [CrossRef]
18. Yan, S.; Wang, H.; Liu, X.; Zu, F.; Liu, D. Effect of the Boundary Layer Low-Level Jet on Fast Fog Spatial Propagation. *Atmos. Chem. Phys.* **2023**, *23*, 13987–14002. [CrossRef]
19. Dhangar, N.; Lal, D.; Ghude, S.; Kulkarni, R.; Parde, A.; Pithani, P.; Niranjan, K.; Prasad, D.; Jena, C.; Sajjan, V.; et al. On the Conditions for Onset and Development of Fog over New Delhi: An Observational Study from the WiFEX. *Pure Appl. Geophys.* **2021**, *178*, 3727–3746. [CrossRef]
20. Shen, P.; Liu, D.; Gultep, I.; Lin, H.; Cai, N.; Cao, S.; Wang, Z. Boundary Layer Features of One Winter Fog in the Yangtze River Delta, China. *Pure Appl. Geophys.* **2022**, *179*, 3463–3480. [CrossRef]
21. Wobrock, W.; Schell, D.; Maser, R.; Kessel, M.; Jaeschke, W.; Fuzzi, S.; Facchini, M.C.; Orsi, G.; Marzorati, A.; Winkler, P.; et al. Meteorological Characteristics of the Po Valley Fog. *Tellus B Chem. Phys. Meteorol.* **1992**, *44*, 469–488. [CrossRef]
22. Pu, M.; Zhang, G.; Yan, W.; Li, Z. Features of a Rare Advection-Radiation Fog Event. *Sci. China Ser. D-Earth Sci.* **2008**, *51*, 1044–1052. [CrossRef]
23. Liu, D.Y.; Niu, S.J.; Yang, J.; Zhao, L.J.; Lü, J.J.; Lu, C.S. Summary of a 4-Year Fog Field Study in Northern Nanjing, Part 1: Fog Boundary Layer. *Pure Appl. Geophys.* **2012**, *169*, 809–819. [CrossRef]
24. Liu, D.Y.; Yan, W.L.; Yang, J.; Pu, M.J.; Niu, S.J.; Li, H.Z. A Study of the Physical Processes of an Advection Fog Boundary Layer. *Bound.-Layer Meteorol.* **2016**, *158*, 125–138. [CrossRef]
25. Ye, X.; Wu, B.; Zhang, H. The Turbulent Structure and Transport in Fog Layers Observed over the Tianjin Area. *Atmos. Res.* **2015**, *153*, 217–234. [CrossRef]
26. Zhou, B.; Ferrier, B. Asymptotic Analysis of Equilibrium in Radiation Fog. *J. Appl. Meteorol. Climatol.* **2008**, *47*, 1704–1722. [CrossRef]
27. Zhang, G.; Bian, L.; Wang, J.; Yang, Y.; Yao, W.; Xu, X. The Boundary Layer Characteristics in the Heavy Fog Formation Process over Beijing and Its Adjacent Areas. *Sci. China Ser. D Earth Sci.* **2005**, *48*, 88–101. [CrossRef]
28. Boutle, I.; Price, J.; Kudzotsa, I.; Kokkola, H.; Romakkaniemi, S. Aerosol–Fog Interaction and the Transition to Well-Mixed Radiation Fog. *Atmos. Chem. Phys.* **2018**, *18*, 7827–7840. [CrossRef]

29. Shao, N.; Lu, C.; Jia, X.; Wang, Y.; Li, Y.; Yin, Y.; Zhu, B.; Zhao, T.; Liu, D.; Niu, S.; et al. Radiation Fog Properties in Two Consecutive Events under Polluted and Clean Conditions in the Yangtze River Delta, China: A Simulation Study. *Atmos. Chem. Phys.* **2023**, *23*, 9873–9890. [CrossRef]
30. Quan, J.; Liu, Y.; Jia, X.; Liu, L.; Dou, Y.; Xin, J.; Seinfeld, J.H. Anthropogenic Aerosols Prolong Fog Lifetime in China. *Environ. Res. Lett.* **2021**, *16*, 044048. [CrossRef]
31. Yan, S.; Zhu, B.; Zhu, T.; Shi, C.; Liu, D.; Kang, H.; Lu, W.; Lu, C. The Effect of Aerosols on Fog Lifetime: Observational Evidence and Model Simulations. *Geophys. Res. Lett.* **2021**, *48*, e2020GL61803. [CrossRef]
32. Pu, M.J.; Ma, M.M.; Zhang, X.R.; Wang, B.N.; Shao, Y.C. An analysis for three successive fogs formation mechanisms in Jiangsu. *J. Meteorol. Sci.* **2018**, *38*, 139–148. (In Chinese) [CrossRef]
33. Wu, B.G.; Zhang, H.S.; Wang, J.; Zhang, C.C.; Yu, L.L.; Liu, B.X.; Xie, Y.Y. Characteristics of the Inversion and the Water VaporTransport during a Duration Fog Event. *Plateau Meteorol.* **2009**, *28*, 258–267. (In Chinese)
34. Zhang, J.; Liu, D.Y.; Qian, Y.Y.; Yan, W.L.; Kang, Z.M. Boundary Layer Features of the Successional Fog and Haze Episode in Jiangsu Area. *J. Arid Meteorol.* **2018**, *36*, 483. Available online: http://www.ghqx.org.cn/CN/10.11755/j.issn.1006-7639(2018)-03-0483 (accessed on 13 April 2026). (In Chinese)
35. Li, T.; Tan, Z.Q.; Ge, S.; Li, Q.; Chao, Y. Formation Mechanism of Local Thick Fog in the Northern Ningxia Hui Autonomous Region on August 22, 2018. *J. Meteorol. Environ.* **2022**, *38*, 8–14. (In Chinese)
36. Tian, H.; Wang, Y.W. Analysis of Climatic Characteristics and Weather Conditions for Fog over the JingJinTang Expressway. *Meteorol. Mon.* **2008**, *34*, 66–71. (In Chinese)
37. Wu, B.G.; Xie, Y.Y.; Wu, D.Z.; Wang, Y.N.; Wang, D.S. Characteristics of Meteorological Elements and Circulation in Fog Events Along Beijing Tianjin Tanggu Expressway. *Meteorol. Mon.* **2010**, *36*, 21–28. (In Chinese)
38. Bao, Y.X.; Ding, Q.J.; Yuan, C.S.; Yan, M.L. Numerical Simulations of a Highly Complex Fog Event on Shanghai-Nanjing Expressway. *Chin. J. Atmos. Sci.* **2013**, *37*, 124–136. (In Chinese) [CrossRef]
39. Yuan, C.S.; Bian, G.H.; Feng, M.X.; Wu, Z.; Zhou, Z.K. Monitoring and Forecasting of Low Visibility on Highways. *Meteorol. Mon.* **2003**, *29*, 36–40. (In Chinese)
40. Ding, Q.J.; Bao, Y.X.; Yuan, C.S.; Yan, M.L. Occurrence pattern and local characteristics of dumpling fog events on Shanghai-Nanjing expressway. *J. Meteorol. Sci.* **2013**, *33*, 634–642. Available online: http://www.jms1980.com//qxkx/article/abstract/20130606 (accessed on 13 April 2026). (In Chinese)
41. Sun, L.Q.; Liu, S.P.; Gao, S.Y.; Cao, S.M.; Wang, W.W.; Fan, X.B. Conditions for sea fog formation in Dandong coast and its synoptic forecasting method. *J. Meteorol. Environ.* **2006**, *22*, 25–28. (In Chinese)
42. Wei, J.S.; Zhu, W.J.; Yan, W.L.; Sun, Y.; Wu, J.; Sun, J.W. Climatic Character is tics of Fog and Its Relevant Influencing Factors over the Coastal Areas of Jiangsu. *Trans. Atmos. Sci.* **2010**, *33*, 680–687. (In Chinese)
43. Wang, B.N.; Pu, M.J.; Tian, L.; Zhang, Z.D.; Wu, J.J. Climate Characteristics and Impact Factors of Low Visibility Heavy Fog on Jiangsu Coast Expressway. *Meteorol. Mon.* **2016**, *42*, 192–202. (In Chinese)
44. Zhang, W.Y.; Sun, X.B.; Li, L.; Zhang, J.Q.; Sun, L.; Qi, X. Climate characteristics and meteorological impact factors of heavy fog along Liaoning coast expressway. *J. Meteorol. Environ.* **2020**, *36*, 67–73. Available online: https://d.wanfangdata.com.cn/periodical/lnqx202001009 (accessed on 13 April 2026). (In Chinese)
45. Dong, H.-P.; Zhao, S.-X.; Zeng, Q.-C. Study of Strong Heavy Rainfall in Low Latitude Plateau Area in China during Early Summer. Part II: Comparison Between Circulation and Climatology Causing Flood in May 2001 and Drought in May 2005. *Clim. Environ. Res.* **2011**, *10*, 460–473. (In Chinese)
46. Cao, J.; Yao, P.; Wang, L.; Liu, K. Summer Rainfall Variability in Low-Latitude Highlands of China and Subtropical Indian Ocean Dipole. *J. Clim.* **2014**, *27*, 880–892. [CrossRef]
47. Hart, R.; Grumm, R. Using Normalized Climatological Anomalies to Rank Synoptic-Scale Events Objectively. *Mon. Weather Rev.* **2001**, *129*, 2426–2442. [CrossRef]
48. Grumm, R.; Hart, R. Standardized Anomalies Applied to Significant Cold Season Weather Events: Preliminary Findings. *Weather Forecast.* **2001**, *16*, 736–754. [CrossRef]
49. Dong, Q.; Sun, J.; Chen, B.; Chen, Y.; Shu, Y. Similarities of Three Most Extreme Precipitation Events in North China. *Atmosphere* **2023**, *14*, 1149. [CrossRef]
50. Ye, H. The Influence of Air Temperature and Atmospheric Circulation on Winter Fog Frequency over Northern Eurasia. *Int. J. Climatol.* **2009**, *29*, 729–734. [CrossRef]
51. Zhang, R.; Li, Q.; Zhang, R. Meteorological Conditions for the Persistent Severe Fog and Haze Event over Eastern China in January 2013. *Sci. China Earth Sci.* **2014**, *57*, 26–35. [CrossRef]
52. Liu, D.; Yang, J.; Niu, S.; Li, Z. On the Evolution and Structure of a Radiation Fog Event in Nanjing. *Adv. Atmos. Sci.* **2011**, *28*, 223–237. [CrossRef]

53. Houssos, E.E.; Lolis, C.J.; Bartzokas, A. The Main Characteristics of Atmospheric Circulation Associated with Fog in Greece. *Nat. Hazards Earth Syst. Sci.* **2009**, *9*, 1857–1869. [CrossRef]
54. Tian, M.; Wu, B.; Huang, H.; Zhang, H.; Zhang, W.; Wang, Z. Impact of Water Vapor Transfer on a Circum-Bohai-Sea Heavy Fog: Observation and Numerical Simulation. *Atmos. Res.* **2019**, *229*, 1–22. [CrossRef]